RSC Advances

ROYAL SOCIETY OF CHEMISTRY

www.rsc.org/advances

Journal Name

ARTICLE

Syntheses, structures, electrochemical and optical properties of four transition metal complexes based on the 1-triazolyl-3-benzimidazolyltriazene ligand

Received 00th January 20xx,
Accepted 00th January 20xx

DOI: 10.1039/x0xx00000x

www.rsc.org/

Yanxuan Qiu, Yu Miao, Zizhou Wang, Zhixin Li, Zhijian OuYang, Liu Yang, Wenning Lin, Weijin Feng and Wen Dong*

Four transition metal complexes based on the 1-triazolyl-3-benzimidazolyltriazene (H_3TBIT) ligand of $[Co(H_2TBIT)(HTBIT)]$ (**1**), $\{[Cu(H_2TBIT)(SCN)]\cdot H_2O\}$ (**2**), $[Cd_2(H_3TBIT)_2(H_2O)_2Cl_4]$ (**3**) and $\{[Ni_3(H_2TBIT)_2(HTBIT)_2(en)_2]\cdot IPA\cdot 2H_2O\}$ (en = ethylenediamine, IPA = isopropanol) (**4**) have been synthesized and characterized by single crystal X-ray diffraction analysis. In **1–4**, the triazene ligand acts in different coordinating or bridging modes resulting in two mononuclear structures for **1** and **2**, one dinuclear structure for **3** and one trinuclear structure for **4**. Different structural **1–4** are further self-assembled through hydrogen bonds or π–π, C–H···π，metal–π interactions to form 3D supramolecular structures. The electrochemical properties in aqueous solutions as well as the photoluminescent properties in ethanol of H_3TBIT and **1–4** are investigated. The TD-DFT calculations at B3LYP/6–311++G(d,p) level for H_3TBIT has been used to demonstrate the characteristic absorption spectrum.

Introduction

Triazenes are a unique type of polyazo compounds including three consecutive nitrogen atoms with a double bond between N1 and N2 (R–N1=N2–N3H–R). They are a very useful and diverse class of compounds and have been used widely in organic syntheses, such as protecting groups for diazonium salts and amines,[1] masking groups in the synthesis of small molecules,[2] alkylating agents for DNA,[3] building blocks for the synthesis of various phenylacetylene-based systems,[4] acting as facilitators of arenes coupling to silicon surfaces,[5] etc. From the viewpoint of coordination chemistry, the triazene group [–N=N–N–] displays a brilliant ability to perform versatility coordination modes with transition metals due to its geometry and electron donor sits, showing a prominent trend to achieve intermolecular, secondary metal-ligand and ligand-ligand interactions and proficient to assemble supramolecular structures.[6] These ligands can serve as monodentate, bidentate, chelate or bridging ligands, as shown in Scheme 1, giving a variety of coordination compounds with large structural diversity.[6a,7] However, their used as ligand in coordination chemistry, compared with related ligands amidinate $[ArNC(R)NAr]^-$,[8] or anionic N–C–X–type (X = N, O, S) ligands,[9] is less developed due to the perceived dangers of handling organic azide compounds and the lack of scalable methods for their preparation.[10] Instead, triazene has been mainly used as a precursor for the triazenide complexes. One the other hand, the studies about triazene complexes are mainly concentrated on their coordination modes and electrochemical properties, seldom attentions are given to their noncovalent interactions and fluorescence properties. With these in mind, we focused our attention on the syntheses, supramolecular structures, electrochemical and optical properties of four transition metal complexes based on the new ligand of 1-triazolyl-3-benzimidazolyltriazene (H_3TBIT).

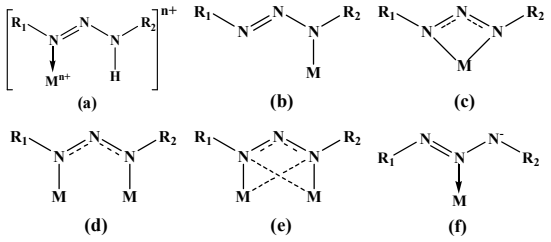

Scheme 1 Main coordination modes of triazenes: (a) neutral monodentate terminal; (b) anionic monodentate terminal; (c) chelating bidentate; (d) bridge-forming; (e) bridge-type syn–syn–η^1:η^1:μ_2; (f) central nitrogen coordination.

School of Chemistry and Chemical Engineering, Guangzhou Key Laboratory for Environmentally Functional Materials and Technology, Guangzhou University, Guangzhou, 510006, China, E-mail: dw320@aliyun.com; Tel: +86-20-31876185; Fax: +86-20-39366902

† Electronic Supplementary Information (ESI) available. See DOI: 10.1039/x0xx00000x

Experimental section

Materials and physical measurements

All the commercial reagents and solvents were purchased and used without further purification unless otherwise stated. ^{1}H NMR and ^{13}C NMR spectra were measured on a 500 MHz Digital NMR Spectrometer (AV III, Ascend 500 HD). IR spectra were recorded as pressed KBr pellets on a Bruker Tensor 27 spectrophotometer with an average of 64 scans. Elemental analyses were carried out using a Perkin–Elmer analyzer model 240. X-ray powder diffraction (XRD) were measured at room temperature using a PANalytical PW3040/60 X-ray diffractometer (Cu-Kα, λ = 1.54056 Å) and the calculated patterns were generated with PowderCell. Thermogravimetric (TG) analyses were carried out using Perkin–Elmer TGA4000 thermogravimetric analyzer. EPR spectrum was acquired on a Bruker ER200-SRC instrument in solid state at room temperature. UV–Vis absorption spectra of H_3TBIT and **1**–**4** in ethanol were collected on a Perkin–Elmer Lambda 750 S UV/VIS/NIR Spectrometer. Cyclic voltammetry experiments were carried out on a CHI–760D electrochemical analyzer using a three-electrode cell, in which a carbon electrode was the working electrode, a platinum plate electrode was the auxiliary electrode, and a saturated calomel electrode (s.c.e) was the reference electrode. For the experiments performed in water as solvent (1×10^{-4} mol·dm^{-3}) containing in 0.01 mol L^{-1} KOH as supporting electrolyte. Luminescence spectra of H_3TBIT and **1**–**4** in ethanol were recorded with a Hitachi F-7000 fluorescence spectrophotometer at room temperature.

X-ray crystallography and data collection

The crystals suitable for X-ray single crystal structural analyses were coated with hydrocarbon oil on the microscope slide and mounted on glass fiber with silicone grease and placed in a Bruker Smart APEX(II) area detector using graphite monochromated Mo–Kα radiation (λ = 0.71073 Å) at 296(2) K. The crystallographic structures were solved by direct methods and successive Fourier difference syntheses (SHELXS-97) and refined by full-matrix least-squares procedure on F^2 with anisotropic thermal parameters for all non-hydrogen atoms (SHELXL-97). Hydrogen atoms were added theoretically and were riding on their parent atoms. The crystal data and collection parameters for **1**–**4** are listed in Table 1.

Computational details

All the quantum-chemical calculations were carried out by the Gaussian09 suit.[11] B3LYP[12] functional is found to perform well for most of the organic molecules, hence the same is employed here. The geometry of H_3TBIT in ground state was optimized using B3LYP functional with 6–311++G(d,p) basis set. The calculated UV–Vis spectrum of H_3TBIT in ethanol was performed using time dependent density functional theory (TD–DFT) at B3LYP/6–311++G(d,p) level.[13]

Preparation of H_3TBIT and complexes 1–4

Synthesis of H_3TBIT. A solution of $NaNO_2$ (1.38 g, 0.02 mol) in 15 mL of water was added dropwise within 20 min to a mixed solution of 3-amino-1,2,4-triazole (1.68 g, 0.02 mol) in 30 mL water and 3 mL of concentrated hydrochloric acid (37%) cooled to 0–5℃. Then a solution of 2-aminobenzimidazole

Table 1 Crystallographic parameters of structures **1–4**

	1	**2**	**3**	**4**
formula	$C_{18}H_{13}CoN_{16}$	$C_{10}H_9CuN_9OS$	$C_{18}H_{20}Cd_2Cl_4N_{16}O_2$	$C_{43}H_{40}N_{36}Ni_3O_5$
Formula weight	512.37	366.87	859.12	1317.18
Crystal system	orthorhombic	monoclinic	monoclinic	monoclinic
Space group	$P2_12_12_1$	$P2_1/n$	$P2_1/c$	$P2_1/n$
a/Å	8.3406(2)	7.061(3)	8.3541(4)	11.7945(11)
b/Å	15.9601(4)	19.716(8)	17.9999(9)	15.2176(14)
c/Å	16.1633(4)	10.302(4)	10.0103(5)	19.0428(18)
α/°	90.00	90.00	90.00	90.00
β/°	90.00	106.146(15)	111.893(2)	105.480(6)
γ/°	90.00	90.00	90.00	90.00
Volume/Å^3	2151.61(9)	1377.6(9)	1396.72(12)	3293.9(5)
Z	4	4	2	2
ρ_{calc}mg/mm^3	1.582	1.769	2.043	1.328
μ/mm^{-1}	0.844	1.754	1.957	0.917
F(000)	1040.0	740.0	840.0	1348.0
Reflections collected	30815	14361	22737	26830
Independent reflections	4971 [R_{int} = 0.0675]	2431 [R_{int} = 0.0632]	3237 [R_{int} = 0.0328]	7938 [R_{int} = 0.0652]
Goodness-of-fit on F^2	0.989	1.142	1.047	0.976
R_1, wR_2[a,b] [I>=2σ(I)]	0.0406, 0.0690	0.0468, 0.1260	0.0207, 0.0483	0.0654, 0.1772
R_1, wR_2[a,b] [all data]	0.0713, 0.0770	0.0667, 0.1613	0.0269, 0.0510	0.1348, 0.2130
CCDC	1422671	1422672	1422673	1428456

[a] $R = \sum||F_o|-|F_c||/\sum|F_o|$. [b] $wR_2 = [\sum w(F_o^2-F_c^2)^2/\sum w(F_o^2)^2]^{1/2}$

(2.66 g, 0.02 mol) in 30 mL ethanol was added slowly to the above mixture solution (Scheme 2a). The resulting mixture was stirred for 24 h at room temperature and a yellow precipitate of H_3TBIT was obtained in 68% yield. The yellow crystals of H_3TBIT were obtained via diffusion method by dissolving crude product of H_3TBIT in N,N-dimethylformamide (DMF) and using isopropanol as diffusion layer. Elemental analysis calcd for $C_9H_8N_8$: C, 47.37; H, 3.51; N, 49.12%. Found: C, 47.24; H, 3.46; N, 49.26%. FT-IR (KBr, cm^{-1}): 3054m, 1637m, 1598m, 1536m, 1488m, 1471m, 1418m, 1353m, 1305m, 1267m, 1234m, 1215m, 1090m, 1073m, 1035m, 1005w, 975m, 887m, 827m, 732m, 635w, 615w, 542w, 496w, 438w. ^{1}H NMR (500 MHz, DMSO-d_6, δ ppm): 13.98 (s, 1H), 13.41 (s, 1H), 8.53 (s, 1H), 7.89 (1H, s), 7.39 (t, J = 4.6, 2H), 7.23 (s, 2H). ^{13}C NMR (500 MHz, DMSO-d_6, δ ppm): 158.43, 131.76, 123.14, 111.99, 99.99, 62.50. MS (ESI) for H_3TBIT m/z $[M-H]^-$ requires: 227.0, found: 227.1. T_d = 186℃ (Fig. S1, ESI†). The reaction mechanisms of diazotization and coupling reaction are given in Scheme 2b. The assembling strategies of complexes **1**–**4** are given in Scheme 2c.

Caution! The preparation of H_3TBIT is potentially explosive and should be handled in small quantities.

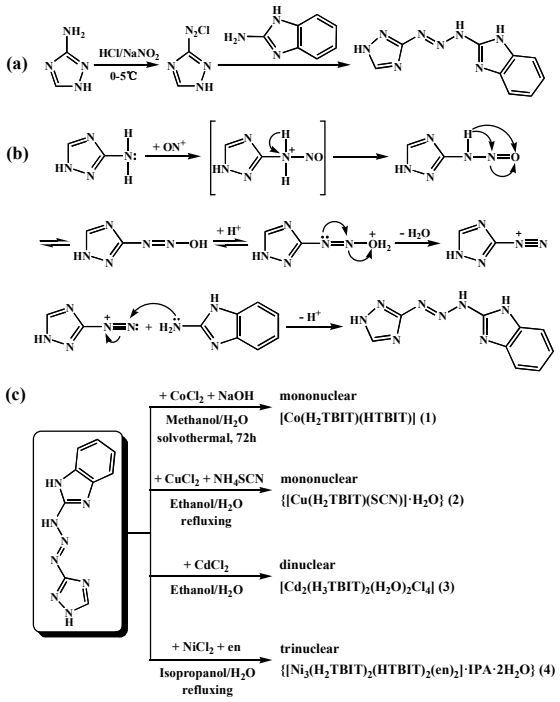

Scheme 2 (a) Synthesis of 1-triazolyl-3-benzimidazolyltriazene (H_3TBIT); (b) the reaction mechanisms of diazotization and coupling reaction; (c) construction of complexes **1**–**4**.

Synthesis of [Co(H_2TBIT)(HTBIT)] (1). A drop of dilute NaOH (2 $mol \cdot L^{-1}$) was added to a solution of 1-triazolyl-3-benzimidazolyltriazene (0.0228 g, 0.1 mmol) in methanol (10 mL) and stirred till the ligand was dissolved. Then a solution of $CoCl_2 \cdot 6H_2O$ (0.0237 g, 0.1 mmol) in water (5 mL) was added to the above solution and stirred for 5 min. The resultant solution was heated in a stainless steel reactor with 25 mL Teflon liner at 100 ℃ for 72 h, followed by slow cooling (5 ℃·h^{-1}) to room temperature. The resulting mixture was filtered and evaporated under ambient conditions. Red crystals of **1** were obtained after one week, isolated by filtration and washed with distilled water. Yield: 36.5% (based on Co^{2+}). Elemental analysis calcd for **1** of $C_{18}H_{13}CoN_{16}$: C, 42.16; H, 2.54; N, 43.72%. Found: C, 42.07; H, 2.58; N, 43.78%. FT-IR (KBr, cm^{-1}): 2652m, 1597w, 1559m, 1483m, 1455m, 1405s, 1357s, 1246m, 1227m, 1196m, 1154m, 1110w, 1076w, 1009w, 951w, 896w, 832w, 743m, 664m, 627w.

Synthesis of {[Cu(H_2TBIT)(SCN)]·H_2O} (2). A mixture of $CuCl_2 \cdot 2H_2O$ (0.0170 g, 0.1 mmol) and NH_4SCN (0.0152 g, 0.2 mmol) in H_2O (5 mL) was added to a solution of 1-triazolyl-3-benzimidazolyltriazene (0.0228 g, 0.1 mmol) in ethanol (10 mL), giving a black solution. The black solution was heated and stirred for 2 hours. After cooling to room temperature, the resulting mixture was filtered and red block crystals of **2** were obtained by slow evaporation under ambient conditions for one day, isolated by filtration and washed with distilled water. Yield: 80.6% (based on Cu^{2+}). Elemental analysis calcd for **2** of $C_{10}H_9CuN_9O_S$: C, 32.71; H, 2.45; N, 34.34%. Found: C, 32.81; H, 2.40; N, 34.43%. FT-IR (KBr, cm^{-1}): 3139m，2284s，1634w，1594w，1556m，1478m, 1455m, 1408s, 1361s, 1336s, 1271m, 1223m, 1176m, 1078m, 974w, 833m, 755m, 660m, 621m, 445w. A single EPR line around 326.474 mT with g = 2.06845 was observed in the solid state at room temperature for **2** (Fig. S2, ESI†).

Synthesis of [Cd_2(H_3TBIT)$_2$(H_2O)$_2$$Cl_4$] (3). 5 mL aqueous solution of $CdCl_2 \cdot 2.5H_2O$ (0.0228 g, 0.1 mmol) was added to a solution of 1-triazolyl-3-benzimidazolyltriazene (0.0228 g, 0.1 mmol) in ethanol (10 mL) and stirred for 2 hours. The resulting mixture was filtered and yellow block crystals of **3** were obtained by slow evaporation of the filtrate after four days and washed with distilled water. Yield: 67.8% (based on Cd^{2+}). Elemental analysis calcd for **3** of $C_{18}H_{20}Cd_2C_{l4}N_{16}O_2$: C, 25.14; H, 2.33; N, 26.07%. Found: C, 25.25; H, 2.28; N, 26.16%. FT-IR (KBr, cm^{-1}): 3362m，1605s, 1514s, 1487m, 1451m, 1409m, 1315s, 1269s, 1212m, 1169m, 1140m, 1084m, 985m, 936m, 887w, 840m, 750w, 669w, 581m, 544w, 494w, 450w.

Synthesis of {[Ni_3(H_2TBIT)$_2$(HTBIT)$_2$(en)$_2$]·IPA·2H_2O} (4). 5 mL aqueous solution of $NiCl_2 \cdot 6H_2O$ (0.0237 g, 0.1 mmol) was

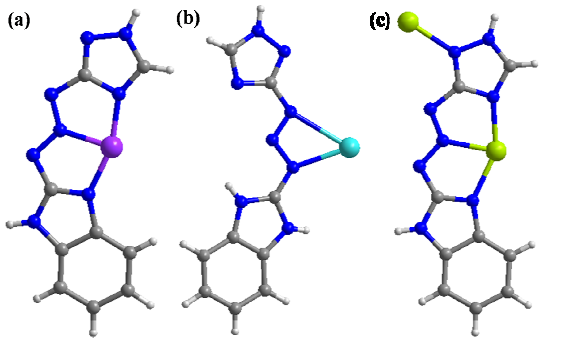

Fig. 1 The coordination modes of H_3TBIT in complexes **1** and **2** (a), **3** (b) and **4** (c).

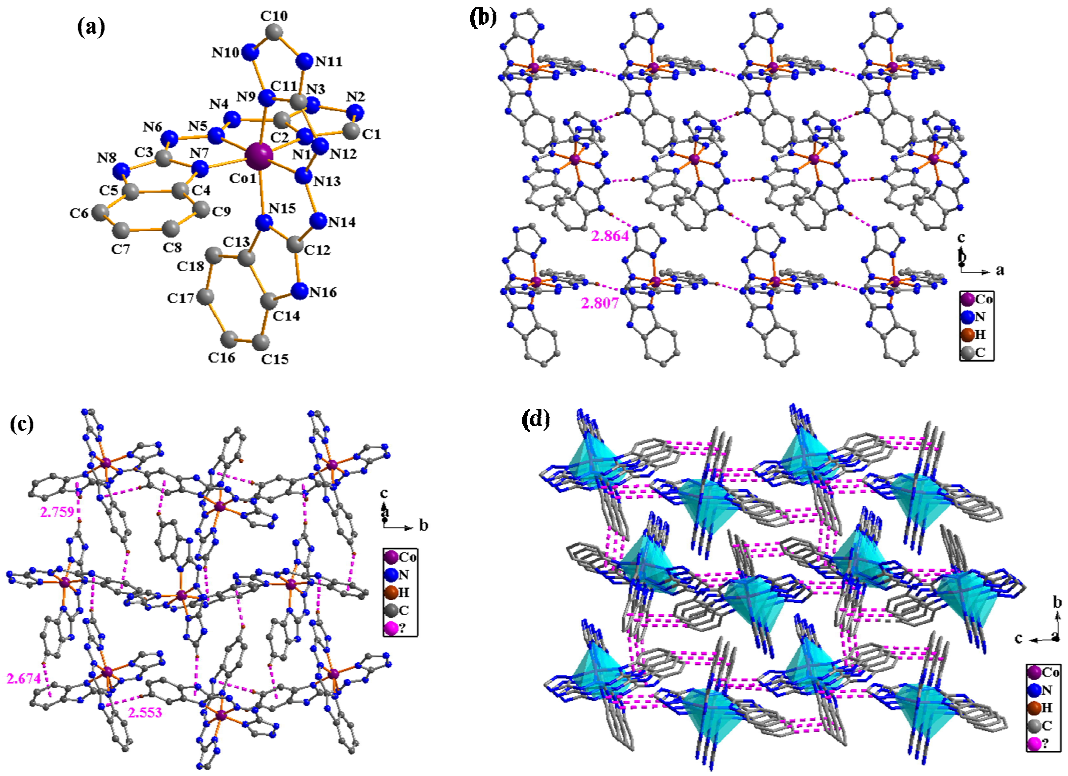

Fig. 2 (a) View of the coordination environments around the Co(III) atom in **1;** (b) the N–H···N hydrogen bonds in **1**, showing a 2D network parallel to the plane *ac*; (c) the C–H···π interaction in **1**, showing another 2D network parallel to the plane *bc*; (d) the 3D supramolecular network of complex **1** via C–H···π contacts. All H atoms except those participating in C–H···π and hydrogen bonds were omitted for clarity.

added to a solution of 1-triazolyl-3-benzimidazolyltriazene (0.0228 g, 0.1 mmol) in 10 mL isopropanol and stirred for 5 min, giving a red solution. To the above mixture, four drops of ethylenediamine was added and then heated and stirred for 4 hours. After cooling to room temperature, the resulting mixture was filtered and red block crystals of **4** were obtained by slow evaporation for two weeks. Yield: 73.4% (based on Ni^{2+}). Elemental analysis calcd for **4** of $C_{43}H_{40}N_{36}Ni_3O_5$: C, 39.17; H, 3.04; N, 38.26%. Found: C, 38.82; H, 3.75; N, 37.93%. FT-IR (KBr, cm^{-1}): 3348m, 1594w, 1525m, 1456m, 1398m, 1343s, 1257w, 1004m, 832w, 746m, 646m, 508w.

Results and discussion

Description of crystal structures

Crystal structure of [Co(H_2TBIT)(HTBIT)] (1). Single-crystal X-ray analysis reveals that complex **1** crystallizes in the orthorhombic with space group $P2_12_12_1$. Complex **1** is a mononuclear structure with each unit cell consisting of one Co^{3+} ion and two anionic ligands of H_2TBIT^- and $HTBIT^{2-}$ (Fig. 2a). Each Co^{3+} coordinates to six nitrogen atoms from two anionic ligands, affording an octahedral geometry. The Co–N bond distances range from 1.8879(23) Å to 1.9198(21) Å, which indicates the Co^{3+} ion.[14] The bond lengths of N4–N5 and N12–N13 are 1.2951(34) Å and 1.2825(36) Å, which are larger than the free ligand calculated by Gaussian09 suite at B3LYP/6–311++G(d,p) level. The free ligand contains a rigid N4=N5 double bond (1.2549 Å). The bond lengths of N5–N6 and N13–N14 are 1.3086(34) Å and 1.3201(36) Å, which are shorter than the free ligand (N5–N6 = 1.3383 Å), owing to the delocalization of the π-electrons in the triazenido moiety (Fig. S3, ESI†). The N4–N5–N6 angle takes a value of 119.20(2)° and the N12–N13–N14 angle value is 118.96(2)°, slightly larger than the free ligand (111.11°). The H_2TBIT^- and $HTBIT^{2-}$ anions act as tridentate chelate ligands (Fig. 1a) and the triazole ring and benzimidazole ring are almost coplanar with the dihedral angle of 2.67° and 5.05°. The intermolecular classical N–H···N hydrogen-bonds among triazenido, triazole and imidazole nitrogen atoms with the shortest distances of N···N = 2.807 Å are present in the crystal structure. It is possible to see that these hydrogen-bonds link the mononuclear structure into a 2D network parallel to plane *ac* (Fig. 2b). At the same time, the C–H···π stacking interactions connect the mononuclear structure into another 2D network parallel to plane *bc* (Fig. 2c). These edge-to-face C–H···π stacking interactions are present between CH groups and aromatic rings with H···π distances of 2.553 Å for C8–H8A···*Cg*1, 2.674 Å for C16–H16A···*Cg*2 (3.5–x, –1–y, –0.5+z) and 2.759 Å for C10–H10···*Cg*3 (3.5–x, –2–y, –0.5+z), in which *Cg*1 and *Cg*3, *Cg*2 are the centriod for the imidazole ring and benzene ring, respectively. As a result, the

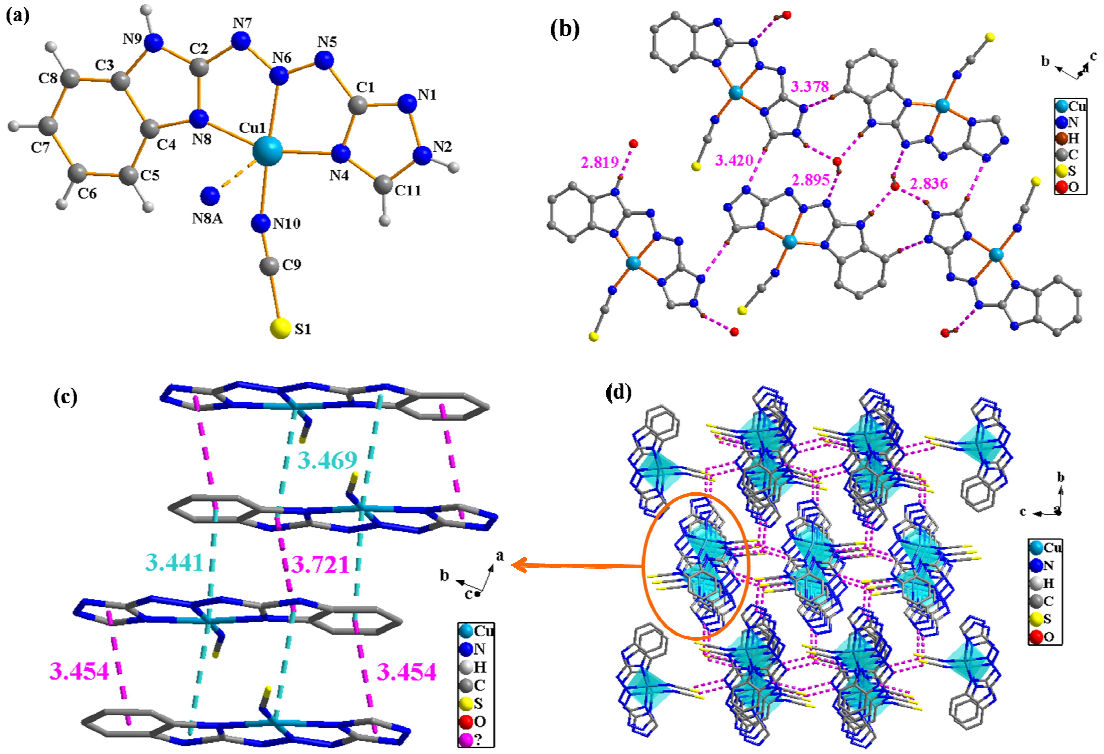

Fig. 3 (a) View of the coordination environments around the Cu(II) atom in **2** (A: 1/2–*x*, 1/2+*y*, 3/2–*z*), uncoordinated water molecules were omitted for clarity; (b) the N–H···O, O–H···N and C–H···N hydrogen bonds in **2**; (c) the face-to-face π–π stacking and metal–π interactions along *a* axis in **2**; (d) the 3D supramolecular frameworks of **2** formed by N–H···O and O–H···N hydrogen bonds, π–π stacking and metal–π interactions. All hydrogen atoms except those participating in the hydrogen bonds were omitted for clarity.

neighboring mononuclear structures are coupled through N–H···N links and C–H···π interactions, thus generating a 3D supramolecular structure (Fig. 2d).

Crystal structure of {[Cu(H_2TBIT)(SCN)]·H_2O} (2). Complex **2** crystallizes in the monoclinic space group $P2_1/n$ with an asymmetric unit that contains one Cu^{2+} ion, one H_2TBIT^- ligand, one SCN^- as ligand and one solvent water molecule. As shown in Fig. 3a, the Cu^{2+} ion is five-coordinated with three nitrogen atoms from one H_2TBIT^- ligand, one nitrogen atom from adjacent H_2TBIT^- ligand and one nitrogen atom from SCN^- anion. The bond lengths of Cu1–N4, Cu1–N6, Cu1–N8, Cu1–N8A and Cu1–N10 are 1.9534(39), 2.0145(40), 1.9523(35), 3.2199(38) and 1.9163(40) Å, respectively. The axial much longer bond length of Cu1–N8A is due to the well-know Jahn–Teller effect for d^9 systems, which afford a serious distorted square pyramidal geometry. The deprotonated ligand leads to a charge delocalization within the triazenido moieties and quite similar N–N bonds (N5–N6 = 1.2832(54) Å, N6–N7 = 1.3053(50) Å) with deviations smaller than 0.03 Å are observed. The N5–N6–N7 angle takes a value of 118.89(37)°, which is quite similar to that found in complex **1** (118.96(2)°). The dihedral angle between triazole ring and benzimidazole ring is 5.66°, indicating a coplanar structure. Solvent water molecule acts both as donor and acceptor of H-bonds with N···O distances ranging 2.819–2.895 Å. These hydrogen bonds together with two non-classic C–H···N hydrogen bonds (C···N = 3.378 and 3.420 Å) link the mononuclear structure into a 2D undulating network parallel to plane *bc* (Fig. 3b). As depicted in Fig. 3c, there are two types of slipped face-to-face π–π stacking interactions found between tridentate chelate ligands that run along *a* axis, forming infinite chains: two equal π–π stacking interactions between triazole ring and benzene ring with center-to-center distances of 3.454 Å, one π–π stacking interactions between imidazole rings with center-to-center distances of 3.721 Å. Within the chains, each Cu^{2+} atom is additionally coordinated by two peripheral aromatic rings of two neighboring complexes by secondary metal–π interaction. These metal–π interactions involve the *Cg*1 (3.469 Å) and *Cg*2 (3.441 Å) with related symmetry code (–x,–y, –z) and (1+x, y, z), respectively. *Cg*1 and *Cg*2 are the centers of imidazole ring and benzene ring, respectively. The adjacent layers parallel to plane *bc* are associated through π–π stacking and metal–π interactions, leading to an overall 3D supramolecular network structure (Fig. 3d).

Crystal structure of [$Cd_2(H_3TBIT)_2(H_2O)_2Cl_4$] (3). X-ray diffraction reveals that complex **3** forms dimer that crystallizes in the monoclinic space group $P2_1/c$ with each unit consisting of two Cd^{2+} ions, two H_3TBIT neutral ligands, four Cl^- as ligand and two coordinated water molecules. Its molecular structure is given in Fig. 4a. Cd1 adopts a distorted octahedral geometry,

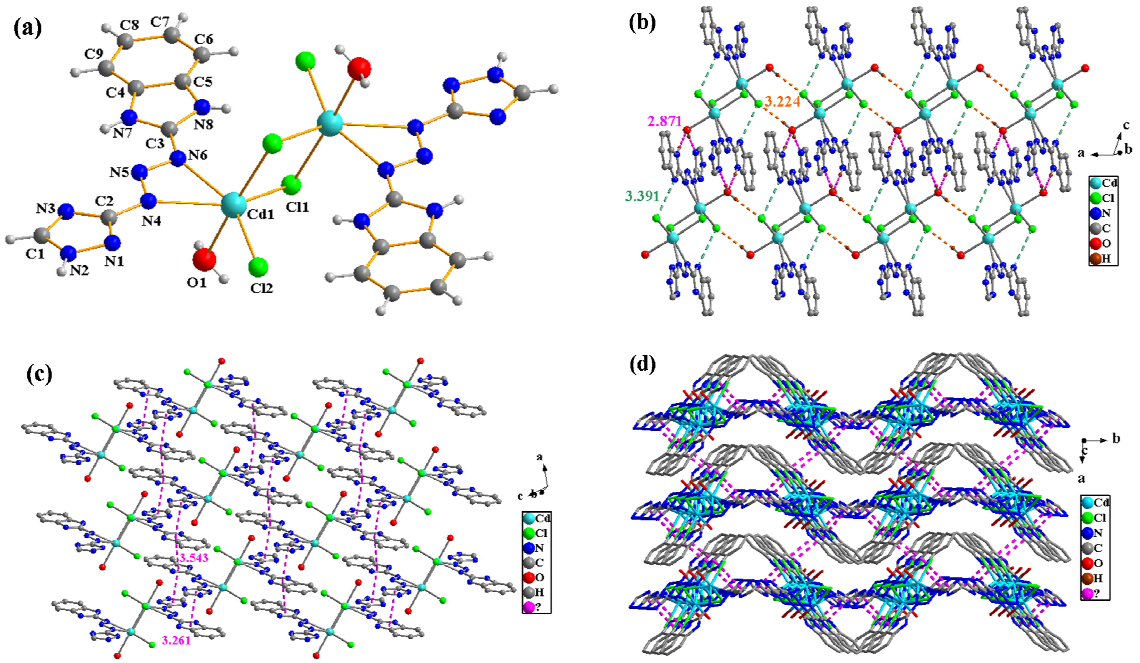

Fig. 4 (a) View of the coordination environments around the Cd(II) atoms in **3**; (b) the O–H···Cl, N–H···Cl, N–H···O and O–H···N hydrogen bonds in **3**; (c) the face-to-face π–π stacking interaction in **3**; (d) 3D supramolecular framework of complex **3** via π–π interactions. All hydrogen atoms except those participating in the hydrogen bonds were omitted for clarity.

coordinating to two nitrogen atoms from one H_3TBIT ligand, to four Cl^-, and one oxygen atom from water molecule. The triazene ligand coordinates to Cd^{2+} in a chelating bidentate way (Fig. 1b). The negative charge of the Cl^- ligands are counter balanced by the central cation Cd^{2+}, and act as bridging ligand coordinating to two different Cd^{2+} ion, resulting in a dinuclear structure with Cd···Cd separation of 3.7352(3) Å. The Cd–N bond lengths are 2.2781(14) and 2.6207(16) Å, the Cd–Cl bond lengths fall in the range of 2.4743(5)–2.6305(6) Å, and the Cd–O bond length is 2.4190(17) Å. The CdN3 metallocycles in **3** possess N–N bond lengths that indicate slight delocalization of charge across the anionic donor (N4–N5 = 1.2723(2) Å, N5–N6 = 1.3356(25) Å) and slight elongation of the Cd–N4 contact. The N4–N5–N6 angle takes a value of 110.09(16)°, which is in accordance with the free ligand (111.11°). There are three types of hydrogen-bonds of O–H···Cl, N–H···Cl and O–H···N among the H_3TBIT neutral ligands, coordinated water molecules and Cl^- ligands with the distances of O···Cl = 3.224 Å, N···Cl = 3.391 Å and O···N = 2.871 Å, showing a 2D network structure (Fig. 4b). Moreover, the H_3TBIT ligands show face-to-face π–π stacking interactions between triazole ring and imidazole ring with separated interplanar center-to-center distance of 3.261 Å, between imidazole rings with separated interplanar center-to-center distance of 3.543 Å (Fig. 4c). The dinuclear structures are connected to 3D supramolecular framework via face-to-face π–π stacking and hydrogen bonding interactions (Fig. 4d).

Crystal structure of {[$Ni_3(H_2TBIT)_2(HTBIT)_2(en)_2$]·IPA·$2H_2O$} (4). X-ray crystallographic study reveals that **4** crystallizes in the monoclinic space group $P2_1/n$. As can be seen in Fig. 5a, the structure of complex **4** consists of three nickel centres, four anionic ligands of H_2TBIT^- and $HTBIT^{2-}$, two en ligands, two solvent water molecules and one isopropanol molecule. Three nickel centres are bridged by two triazenido ligands (Fig. 1c), appearing two different coordination environments, Ni1 is six-coordinated by six nitrogen atoms from one H_2TBIT^- and one $HTBIT^{2-}$ anionic ligands. The Ni1–N bond distances fall in the range 2.054(5)–2.0957(53) Å, adopting a slightly distorted octahedral geometry. Ni2 is six-coordinated by two nitrogen atoms from two $HTBIT^{2-}$ and four nitrogen atoms from two en molecules. The Ni2–N bond distance of triazenido ligands is 2.0962(61) Å, the distances between nickel and nitrogen atom of en are 2.1056(59) Å and 2.0797(72) Å. The average N4–N5/N13–N12 and N5–N6/N12–N11 bond lengths of 1.2807 and 1.3221 Å also imply a delocalization of π electrons in the triazenido chains. Three N–H···N, O–H···O and O–H···N hydrogen bonding interactions are found among H_2TBIT^- and $HTBIT^{2-}$ anionic ligands, solvent water molecules and isopropanol molecules with the shortest distances of N···N = 2.849 Å, O···O = 2.569 Å and O···N = 2.781 Å (Fig. 5b). Fig 5c gives the 3D supramolecular framework formed by hydrogen bonds.

XRD and thermal stability analyses

The XRD measurements were carried out at room temperature to confirm the phase purity of complexes **1**–**4**. As shown in Fig. S4,† the peak positions of experimental XRD patterns are in

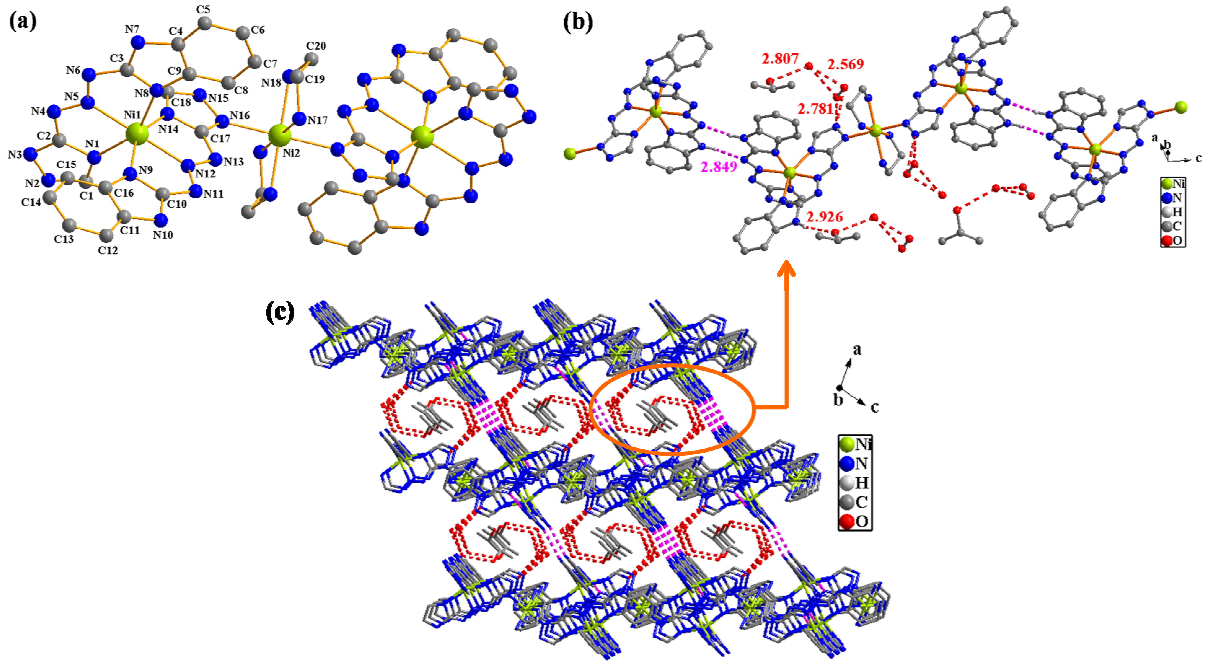

Fig. 5 (a) View of the coordination environments around the Ni(II) atoms in **4**, all H atoms and uncoordinated water molecules were omitted for clarity; (b) the N–H···N, O–H···O and O–H···N hydrogen bonds in **4**; (c) 3D supramolecular framework of complex **4** via hydrogen bonds interactions. All hydrogen atoms except those participating in the hydrogen bonds were omitted for clarity.

agreement with the simulated XRPD patterns, demonstrating the good phase purity of the four complexes.

In order to examine the thermal stabilities of the four complexes, the thermal gravimetric (TG) analyses were carried out in the temperature range of 30–700℃ under a flow of nitrogen with heating rate of 20 ℃·min^{-1} (Fig. 6). For complex **1**, there is no obvious weight loss before 367℃ and then the network decomposes rapidly on further heating. Complex **2** loses the lattice water molecules (calcd 4.9% and expt 4.8%) at the beginning from 86℃ to 137℃. The structure is stable between 137℃ to 240℃ and then undergoes decomposition after 240℃. For complex **3**, the frame structure is stable before 196℃ and then it decomposes rapidly on further heating. For complex **4**, the first weight loss of 7.1% from 70℃ to 130℃ corresponds to the loss of two lattice water molecules and one isopropanol molecule (calcd 7.3%) of one unit cell. The network decomposes in the temperature range 290℃ to 530℃, indicating the thermally stable property of **4** over a broad temperature range. The observed weight losses contain two steps between 290℃ and 530℃, which can be attributed to the elimination of ethylenediamine and H_3TBIT ligands.

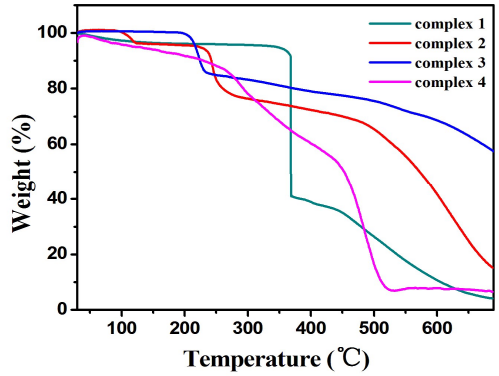

Fig. 6 Thermal gravimetric analyses (TGA) curves for complexes **1–4.**

The UV–Vis absorption of H_3TBIT and 1–4

UV–Vis spectra of H_3TBIT and **1**–**4** in ethanol solutions with the concentration of 1 × 10^{-4} mol·dm^{-3} as well as the calculated electronic spectrum for H_3TBIT have been measured. Calculations of molecular orbital geometry show that the visible absorption maxima of this kind of triazenes correspond to the electron transition from HOMO to LUMO.[15] The experimental and calculated absorption maxima for H_3TBIT are in agreement within the accuracy of the computational method used. As illustrated in Fig. 7a, ligand H_3TBIT has three obvious absorption peaks centered at 207 nm, 269 nm and 367 nm, while the calculated absorption peaks are located in 203 nm, 261 nm and 364 nm, which are in accordance with experimental values. The absorption peak at 203 nm involves mainly a transition from molecular orbital (MO) 58 (HOMO–1) to LUMO+4 (MO = 64) with oscillator strength f = 0.3671, the absorption peak at 261 nm is attributed to HOMO–2 (MO = 57) → LUMO (MO = 60) with oscillator strength f = 0.3688 and the band at 364 nm is assigned as HOMO (MO = 59) → LUMO (MO = 60) with oscillator strength f = 0.7153 (Fig. 7b). The UV–Vis

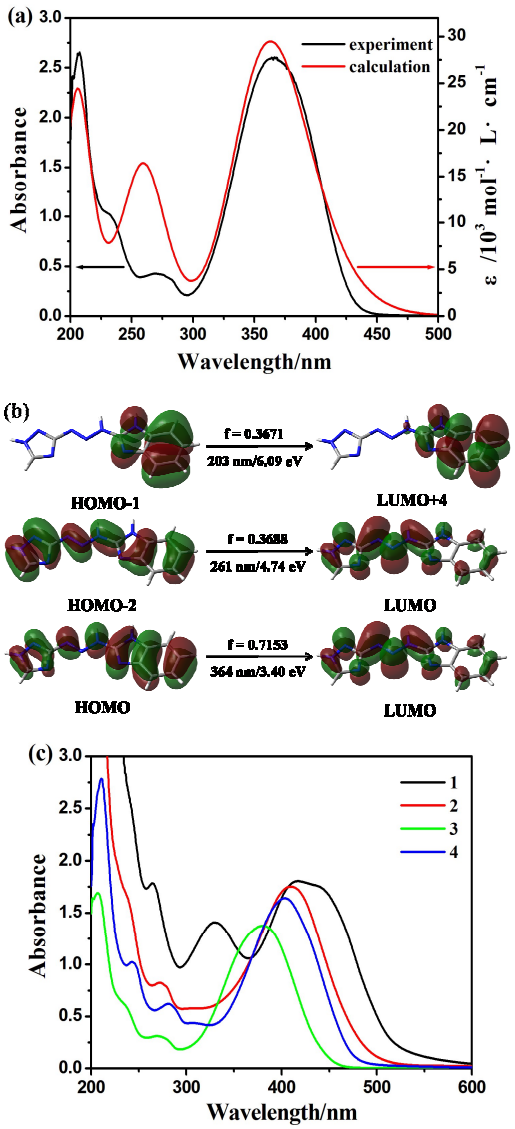

Fig. 7 (a) The experimental and calculated absorption spectra for H_3TBIT in ethanol; (b) the molecular orbitals involved in the main electronic transitions for H_3TBIT in ethanol obtained from DFT calculations; (c) the UV–Vis spectra for ethanol solutions of **1–4** at room temperature.

spectra for **1**–**4** are given in Fig. 7c. Compared with H_3TBIT, the absorption maxima of low-energy bands of complexes **1** (417 nm), **2** (408 nm), **3** (380 nm) and **4** (404 nm) are red-shifted to a longer–wavelength region. This is assignable to spin–orbit coupling from the heavy atom effect of the transition metal ions as well as a M→L MLCT transition upon deprotonated H_3TBIT binding to the transition metal ions.[16]

Cyclic voltammetry for H_3TBIT and 1–4

The redox activity of H_3TBIT and **1**–**4** are studied in aqueous solution (0.01 mol·dm^{-3} in KOH) using cyclic voltammetry on the positive side at a carbon working electrode. Results are collected in Fig. 8. Cyclic voltammogram of H_3TBIT in water displays only one pair of redox peaks, which can be attributed to the formation of triazene cation radical intermediates and then protonation with residual water rearranges secondary amines.[17] Cyclic voltammogram of complexes **1**–**3** also exhibit one pair of redox peaks, which can be ascribed to the $Co^{III/II}$, $Cu^{II/I}$ and $Cd^{II/I}$ processes, respectively, as the triazene ligand without hydrogen in complexes do not form radical adducts during the electrochemical reduction.[17] These are irreversible one-electron redox couples with ΔE = 160 mV and i_a/i_c = 1.035 for H_3TBIT, ΔE = 140 mV and i_a/i_c = 0.938 for **1**, ΔE = 400 mV and i_a/i_c = 0.669 for **2**, ΔE = 280 mV and i_a/i_c = 0.638 for **3** (i_a and i_c are the anodic and cathodic currents, respectively). However, complex **4** shows two oxidation waves and one cathodic wave (Fig. 8e). The anodic peaks potentials at 50 mV·s^{-1} for these waves are at E_l = 0.925 V and E_2 = 1.575 V and the cathodic peak potential is −0.575 V.

The photoluminescence for H_3TBIT and 1–4

The fluorescence properties of the triazene ligand H_3TBIT together with its transition metal complexes **1**–**4** are studied at room temperature in ethanol solution (1 × 10^{-4} mol·dm^{-3}, Fig. 9). The free ligand H_3TBIT displays photoluminescence with emission maximum at 438 nm upon excitation at 299 nm, which can probably be attributed to π → π* or n → π* transitions. Complex **1** shows an intense blue fluorescent emission with maximum and shoulder bands at 428 and 408 nm under 369 nm light excitation, and complex **3** displays an intense emission with maximum and shoulder bands at 432 nm and 453 nm upon 354 nm light excitation, which may

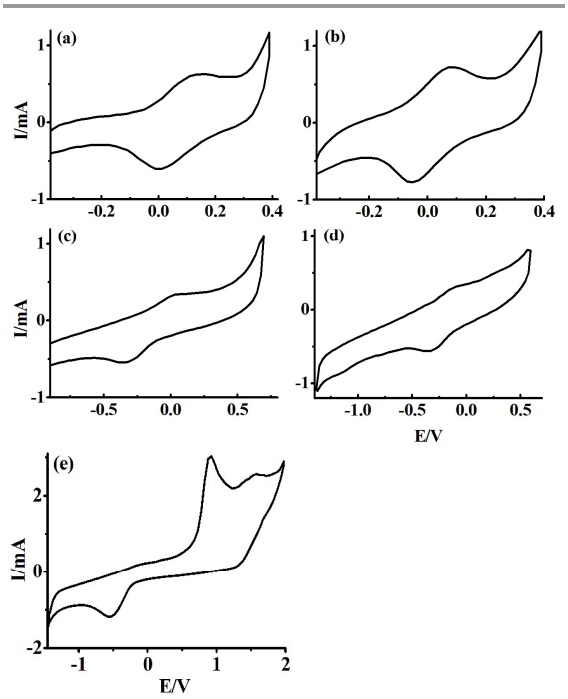

Fig. 8 Cyclic voltammetry of H_3TBIT (a), **1** (b), **2** (c), **3** (d) and **4** (e) in water (1 × 10^{-4} mol·dm^{-3}, 0.01 mol·dm^{-3} KOH) at carbon working electrode with scan rate of 30 mV·s^{-1} for H_3TBIT and **1–3** and 50 mV·s^{-1} for **4**.

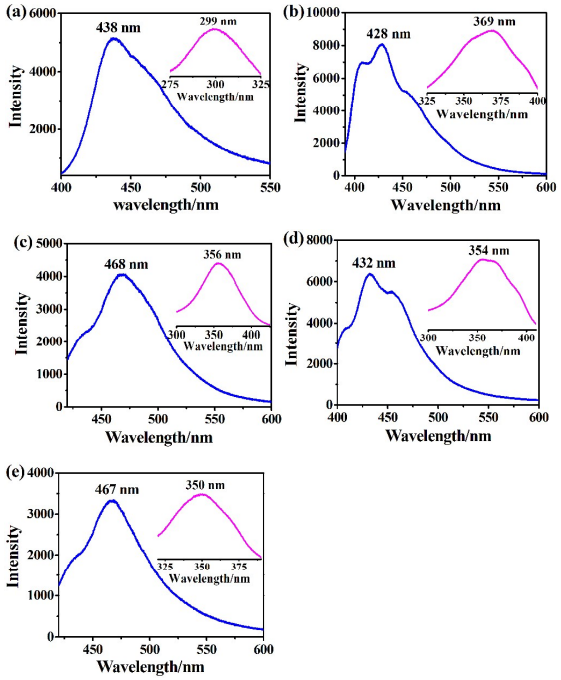

Fig. 9 Room-temperature emission spectra of H_3TBIT (a), **1** (b), **2** (c), **3** (d) and **4** (e) in ethanol with the concentration of 1×10^{-4} mol·dm^{-3}. Insets are their corresponding excitation spectra.

probably be attributed to the intraligand charge transitions.[18] Irradiation of complex **2** at 356 nm results in red-shife emission band at 468 nm. Also, irradiation of complex **4** at 350 nm results in red-shife emission band at 467 nm. The large red-shift emissions at 468 nm for **2** and 467 nm for **4** compared with the emission band of H_3TBIT at 438 nm could be assigned to the metal-perturbed intraligand charge transfer.[18] The observed blue and red shift of the emission bands between complexes **1**–**4** could be assigned to the difference in the nature of Co(III), Cu(II), Cd(II) and Ni(II), the influence of the coordination of the metal ions to the ligand, and the influence of second ligands.[19]

Conclusions

In conclusion, four transition metal complexes based on the new ligand of H_3TBIT have been synthesized and reported. The H_3TBIT has both π-system capable of forming π–π stacking, C–H···π and metal–π interactions and the ability for formation of intermolecular classical and non-classic hydrogen bonds. The structural diversification illustrates that the non-covalent interactions seems to play an important role in the crystal packing and the formation of the framework. The electrochemical and optical properties of these complexes were analysed and demonstrated. This study suggests that H_3TBIT is a suitable ligand for the synthesis of multinuclear metal complexes, its complexes are good candidates for potential inorganic-organic hybrid photoactive materials.

Acknowledgements

This work was supported by the National Natural Science Foundation of China (No. 21271052), Science and Technology Program Foundation of Guangdong (No. 2015A030313502) and Program Foundation of the second batch of innovation teams of Guangzhou Bureau of Education (13C04).

Notes and references

1 (a) M. L. Gross, D. H. Blank and W. M. Welch, *J. Org. Chem.*, 1993, **58**, 2104; (b) H. Jian and J. M. Tour, *J. Org. Chem.*, 2005, **70**, 3396.

2 (a) K. C. Nicolau, C. N. C. Boddy, H. Li, A. E. Koumbis, R. Hughes, S. Natarajan, N. F. Jain, J. M. Ramanjulu, S. Bräse and M. Soloman, *Chem. Eur. J.*, 1999, **5**, 2602; (b) C. Torres-García, D. Pulido, F. Albericio, M. Royo and E. Nicolás, *J. Org. Chem.*, 2012, **77**, 9852; (c) C. Torres-García, D. Pulido, M. Carceller, I. Ramos, M. Royo and E. Nicolás, *J. Org. Chem.*, 2014, **79**, 11409.

3 (a) C. A. Rouzer, M. Sabourin, T. L. Skinner, E. J. Thompson, T. O. Wood, G. N. Chmurny, J. R. Klose, J. M. Roman, R. H., Jr. Smith and C. J. Michejda, *Chem. Res. Toxicol.*, 1996, **9**, 172; (b) F. Marchesi, M. Turriziani, G. Tortorelli, G. Avvisati, F. Torino and L. De Vecchis, *Pharmacol. Res.*, 2007, **56**, 275; (c) Z. Rachid, F. Brahimi, Q. Qiu, C. Williams, J. M. Hartley, J. A. Hartley and B. J. Jean-Claude, *J. Med. Chem.*, 2007, **50**, 2605.

4 D. B. Kimball and M. M. Haley, *Angew. Chem., Int. Ed.*, 2002, **41**, 3338.

5 B. Chen, A. K. Flatt, H. Jian, J. L. Hudson and J. M. Tour, *Chem. Mater.*, 2005, **17**, 4832.

6 (a) D. F. Back, M. Hörner, F. Broch and G. M. de Oliveira, *Polyhedron*, 2012, **31**, 558; (b) M. Hörner, G. Manzoni de Oliveira, J. S. Oliveira, W. M. Teles, C. A. L. Filgueiras and J. Beck, *J. Organomet. Chem.*, 2006, **691**, 251; (c) M. Hörner, G. Manzoni de Oliveira, J. S. Bonini and H. Fenner, *J. Organomet. Chem.*, 2006, **691**, 655; (d) A. S. Peregudov, D. N. Kravtso, G. I. Drogunova, Z. A. Starikova and A. I. Yanovsky, *J. Organomet. Chem.*, 2000, **597**, 164.

7 (a) X. H. Xie, J. Y. Chen, W. Q. Xu, E. X. He and S. Z. Zhan, *Inorganica. Chimica. Acta.*, 2011, **373**, 276; (b) D. B. Kimball and M. M. Haley, *Angew. Chem., Int. Ed.*, 2002, **41**, 3338; (c) M. K. Rofouei, Z, Ghalami, J. A. Gharamaleki, V. Ghoulipour, G.Bruno and H. A. Rudbari, *Z. Anorg. Allg. Chem.*, 2012, **638**, 798; (d) M. K. Rofouei, J. A. Gharamaleki, E. Fereyduni, A. Aghaei, G. Bruno and H. A. Rudbari, *Z. Anorg. Allg. Chem.*, 2012, **638**, 220.

8 (a) F. T. Edelmann, *Coord. Chem. Rev.*, 1994, **137**, 403; (b) J. Barker and M. Kilner, *Coord. Chem. Rev.*, 1994, **133**, 219; (c) L. A. Oro, M. A. Ciriano, J. J. Perez-Torrente and B. E. Villaroya, *Coord. Chem. Rev.*, 1999, **193–195**, 941.

9 Z. Z. Zhang and H. Cheng, *Coord. Chem. Rev.*, 1996, **147**, 1.

10 (a) W. J. Lei, X. W. Tan, L. J. Han, S. Z. Zhan and B. T. Li, *Inorg. Chem. Commun.*, 2010, **13**, 1325; (b) H. C. Kolb, M. G. Finn and K. B. Sharpless, *Angew. Chem. Int. Ed.*, 2001, **40**, 2004; (c) S. G. Alexander, M. L. Cole, C. M. Forsyth, S. K. Furfari and K. Konstas, *Dalton Trans.*, 2009, 2326.

11 M. J. Frisch, G. W. Trucks, H. B. Schlegel, G. E. Scuseria, M. A. Robb, J. R. Cheeseman, G. Scalmani, V. Barone, B. Mennucci, G. A. Petersson, H. Nakatsuji, M. Caricato, X. Li, H. P. Hratchian, A. F. Izmaylov, J. Bloino, G. Zheng, J. L. Sonnenberg, M. Hada, M. Ehara, K. Toyota, R. Fukuda, J. Hasegawa, M. Ishida, T. Nakajima, Y. Honda, O. Kitao, H. Nakai, T. Vreven, J. A. Montgomery Jr, J. E. Peralta, F. Ogliaro, M. Bearpark, J. J. Heyd, E. Brothers, K. N. Kudin, V. N. Staroverov, R. Kobayashi, J. Normand, K. Raghavachari, A. Rendell, J. C. Burant, S. S. Iyengar, J. Tomasi, M. Cossi, N.

Rega, J. M. Millam, M. Klene, J. E. Knox, J. B. Cross, V. Bakken, C. Adamo, J. Jaramillo, R. Gomperts, R. E. Stratmann, O. Yazyev, A. J. Austin, R. Cammi, C. Pomelli, J. W. Ochterski, R. L. Martin, K. Morokuma, V. G. Zakrzewski, G. A. Voth, P. Salvador, J. J. Dannenberg, S. Dapprich, A. D. Daniels, O. Farkas, J. B. Foresman, J. V. Ortiz, J. Cioslowski and D. J. Fox, *GAUSSIAN 09 (Revision A. 02)*, Gaussian, Inc., Wallingford, CT, 2009.

12 (a) A. D. Becke, *J. Chem. Phys.*, 1993, **98**, 5648; (b) C. Lee, W. Yang, R. G. Parr, *Phys. Rev. B*, 1988, **37**, 785.

13 J. J. Jiang, C. Yan, M. Pan, Z. Wang, H. Y. Deng, J. R. He, Q. Y. Yang, L. Fu, X. F. Xu and C. Y. Su, *Eur. J. Inorg. Chem.*, 2012, 1171.

14 (a) W. Addison, T. N. Rao, J. Reedijk, J. Rijn and G. C. Verschoor, *J. Chem. Soc., Dalton Trans.*, 1984, 1349; (b) J. M. Lin, B. S. Huang, Z. Q. Liu, D. Y. Wang and W. Dong, *CrystEngComm*, 2009, **11**, 329.

15 H. A. Dabbagh, A. Teimouri, A. N. Chermahini and R. Shiasi, *Spectrochimica Acta Part A*, 2007, **67**, 437.

16 H. M. Wen, Y. H. Wu, Y. Fan, L. Y. Zhang, C. N. Chen and Z. N. Chen, *Inorg. Chem.*, 2010, **49**, 2210.

17 P. Rapta, L. Omelka, A. Stasko, J. Dauth, B. Deubzer and J. Weis, *J. Chem. Soc., Perkin Trans. 2*, 1996, 255.

18 S. Q. Zhang, F. L. Jiang, M. Y. Wu, L. Chen, J. H. Luo and M. C. Hong, *CrystEngComm*, 2013, **15**, 3992.

19 S. Y. Song, X. Z. Song, S. N. Zhao, C. Qin, S. Q. Su, M. Zhu, Z. M. Hao and H. J. Zhang, *Dalton Trans.*, 2012, **41**, 10412.

The crystal structures, electrochemical and optical properties of four transition metal complexes based on 1-triazolyl-3-benzimidazolyltriazene (H_3TBIT) ligand have been reported.